THE JOURNAL OF BIOLOGICAL CHEMISTRY VOL. 287, NO. 47, pp. 39460–39469, November 16, 2012
© 2012 by The American Society for Biochemistry and Molecular Biology, Inc. Published in the U.S.A.

Distinct Roles of the C-terminal 11th Transmembrane Helix and Luminal Extension in the Partial Reactions Determining the High Ca^{2+} Affinity of Sarco(endo)plasmic Reticulum Ca^{2+}-ATPase Isoform 2b (SERCA2b)*

Received for publication, July 2, 2012, and in revised form, September 19, 2012 Published, JBC Papers in Press, September 28, 2012, DOI 10.1074/jbc.M112.397331

Johannes D. Clausen[‡§], **Ilse Vandecaetsbeek**[¶], **Frank Wuytack**[¶], **Peter Vangheluwe**[¶1], **and Jens Peter Andersen**[‡2]

From the Departments of [‡]*Biomedicine and* [§]*Molecular Biology and Genetics, Centre for Membrane Pumps in Cells and Disease, PUMPKIN, Danish National Research Foundation, Aarhus University, DK-8000 Aarhus C, Denmark and the* [¶]*Laboratory of Cellular Transport Systems, Department of Cellular and Molecular Medicine, KU Leuven, B-3000 Leuven, Belgium*

Background: Little is known about the mechanism by which the luminal extension (LE) and 11th transmembrane helix (TM11) of SERCA2b regulate function.
Results: Mutant and chimeric SERCA constructs were analyzed kinetically.
Conclusion: The LE affects Ca^{2+} interaction in *E*1 and *E*1P, whereas TM11 affects Ca^{2+}-free *E*2/*E*2P states.
Significance: Distinct roles of LE and TM11 in controlling the enzyme cycle are revealed.

The molecular mechanism underlying the characteristic high apparent Ca^{2+} affinity of SERCA2b relative to SERCA1a and SERCA2a isoforms was studied. The C-terminal tail of SERCA2b consists of an 11th transmembrane helix (TM11) with an associated 11-amino acid luminal extension (LE). The effects of each of these parts and their interactions with the SERCA environment were examined by transient kinetic analysis of the partial reaction steps in the Ca^{2+} transport cycle in mutant and chimeric Ca^{2+}-ATPase constructs. Manipulations to the LE of SERCA2b markedly increased the rate of Ca^{2+} dissociation from Ca_2E1. Addition of the SERCA2b tail to SERCA1a slowed Ca^{2+} dissociation, but only when the luminal L7/8 loop of SERCA1 was simultaneously replaced with that of SERCA2, thus suggesting that the LE interacts with L7/8 in Ca_2E1. The interaction of LE with L7/8 is also important for the low rate of the $Ca_2E1P \rightarrow E2P$ conformational transition. These findings can be rationalized in terms of stabilization of the Ca_2E1 and Ca_2E1P forms by docking of the LE near L7/8. By contrast, low rates of *E*2P dephosphorylation and $E2 \rightarrow E1$ transition in SERCA2b depend critically on TM11, particularly in a SERCA2 environment, but do not at all depend on the LE or L7/8. This indicates that interaction of TM11 with SERCA2-specific sequence element(s) elsewhere in the structure is critical in the Ca^{2+}-free *E*2/*E*2P states. Collectively these properties ensure a higher Ca^{2+} affinity of SERCA2b relative to other SERCA isoforms, not only on the cytosolic side, but also on the luminal side.

Active removal of Ca^{2+} from the cytosol is a critical aspect of signal transduction pathways in animal cells, facilitating the rapid cytosolic Ca^{2+} oscillations required for a wide range of physiological functions such as muscle contraction, neuronal transmission, cellular motility, and cell growth. By coupling the hydrolysis of ATP with the transport of Ca^{2+} ions across the endoplasmic reticulum membrane, the Ca^{2+}-ATPase of sarco-(endo)plasmic reticulum (SERCA)[3] is an important player in the control of the intracellular Ca^{2+} concentration.

The human genome contains three SERCA genes, *ATP2A1*, *ATP2A2*, and *ATP2A3*, encoding SERCA1, SERCA2, and SERCA3 proteins, respectively. Through tissue-specific and developmentally regulated alternative splicing, each of the three genes gives rise to 2–6 splice variants with differing carboxyl termini. The SERCAs are thought to accomplish Ca^{2+} transport by a reaction cycle (Scheme 1) involving the sequential formation and decay of an aspartyl-phosphorylated intermediate, coupled to changes in the Ca^{2+} binding sites, altering between states that are either directed toward the cytosol, tightly occluded inside the protein, or directed toward the endoplasmic reticulum lumen. A change in affinity, being high toward the cytosolic side and low toward the luminal side, facilitates the unidirectional translocation of Ca^{2+} against a large Ca^{2+} gradient. Crystal structures of the SERCA1a isoform have demonstrated that the cytoplasmic N ("nucleotide binding"), P ("phosphorylation"), and A ("actuator") domains undergo large rearrangements during the phosphoenzyme processing steps, which are transformed into both translational and rotational movements of transmembrane helices containing Ca^{2+} binding amino acid residues (1, 2).

The residues making up the Ca^{2+} sites in the transmembrane region are conserved among the SERCA isoforms, being located in transmembrane segments M4, M5, M6, and M8. All of the

* This work was supported in part by grants from the Lundbeck Foundation (to J. D. C.), the Danish Medical Research Council (to J. P. A.), the Novo Nordisk Foundation (to J. P. A.), the Danish National Research Foundation (PUMPKIN Centre), Research Program of the Flanders Research Foundation (FWO-Vlaanderen) Grants G.0646.08 and G.0442.12, and the Interuniversity Attraction Poles Program P6/28 of the Belgian State, Federal Office for Scientific Technical and Cultural Affairs.
[1] Postdoctoral fellow of the Flanders Research Foundation (FWO-Vlaanderen).
[2] To whom correspondence should be addressed: Ole Worms Allé 4, Bldg. 1160, DK-8000 Aarhus C, Denmark. E-mail: jpa@fi.au.dk.

[3] The abbreviations used are: SERCA, sarco(endo)plasmic reticulum Ca^{2+}-ATPase; LE, the 11-amino acid luminal extension; TM1–TM11, the 11 transmembrane segments numbered from the NH_2-terminal end of the protein; T1032*, amino acid T1032 followed by STOP condon indicated as asterisk.

SERCA isoforms, with the exception of the ubiquitously expressed SERCA2b, possess a total of 10 transmembrane segments. The SERCA2b enzyme contains a 49-amino acid C-terminal extension ("the SERCA2b tail," Fig. 1) that makes up an 11th transmembrane helix (TM11) continuing into an 11-amino acid luminal extension (LE) (3–7). Analysis of the Ca^{2+} dependence of Ca^{2+} transport and ATPase activity at steady state has demonstrated that SERCA2b exhibits markedly higher apparent affinity for cytosolic Ca^{2+} and lower maximal transport activity than any other SERCA isoform (4, 6, 8–12). Both TM11 and the LE of SERCA2b have in steady-state measurements of the Ca^{2+} dependence of ATPase activity been found critical to the higher apparent Ca^{2+} affinity of SERCA2b. Hence, deletion of the LE of SERCA2b resulted in a significant lowering of the apparent affinity for cytosolic Ca^{2+} (6, 8), and supplementation of SERCA1a with a synthetic peptide corresponding to either the LE (6) or TM11 (7) increased the apparent Ca^{2+} affinity. In the LE region, particularly the last four residues ^{1039}MFWS appeared important (6).

Little is, however, known about the mechanisms by which the various parts of the SERCA2b tail exert a regulatory effect. Dode *et al.* (10) showed that the SERCA2b tail as a whole is critical for the rates of several partial reaction steps in the enzyme cycle, including the dissociation of Ca^{2+} toward the cytoplasmic side from Ca_2E1, the phosphoenzyme processing reaction sequence $Ca_2E1P \rightarrow E2P \rightarrow E2$, and the Ca^{2+} binding transition, $E2 \rightarrow E1 \rightarrow Ca_2E1$. The apparent affinity for Ca^{2+} activation of the overall reaction depends not only on the "true" Ca^{2+} affinity (*i.e.* the on and off rates of Ca^{2+} at the $E1$ sites), but in addition rate constants of the $Ca_2E1P \rightarrow E2P$ and $E2 \rightarrow E1$ conformational transitions that limit the overall rate of the cycle are critical determinants of the apparent Ca^{2+} affinity, as has been demonstrated both experimentally and in a series of computer simulations of the cycle (13). This raises the question whether TM11 and the LE affect the same or distinct partial reactions of the enzyme cycle, and which ones? This question was not addressed in the previous studies focusing on the functional regions of the SERCA2b tail in studies of the overall reaction and its Ca^{2+} dependence. Information about effects on the individual partial reactions by the various parts of the tail is crucial to the understanding of when in the cycle, and how, physical interaction takes place between the tail and the protein, and is thus a key point in the elucidation of the mechanism(s) underlying the regulatory effects exerted by the tail.

Hence, in the present study we set out to investigate these matters in transient kinetic studies of the differential effects of the TM11 and LE on individual partial reactions of the enzyme cycle. On the one hand, we studied mutants with alterations to either the TM11 or LE, which were previously reported to display a loss of SERCA2b tail function with respect to the apparent Ca^{2+} affinity determined for the overall reaction (6). On the other hand, we followed a gain of function approach by characterizing the kinetics of SERCA1a-2b chimeras in which the SERCA2b tail is gradually reconstructed in the SERCA1a background. Using this combined approach we show that the LE is the most important determinant of the dissociation of Ca^{2+} from the Ca_2E1 form, whereas TM11 is of particular importance for the rates of the $E2P \rightarrow E2$ and $E2 \rightarrow E1$ partial reaction steps. A critical interaction of TM11 with SERCA2 specific component(s) appears to be involved in the $E2$/$E2P$ states.

EXPERIMENTAL PROCEDURES

The cDNA encoding the wild types or various SERCA constructs studied in the present work was either the same as in previous studies (6, 10) or was newly prepared using the methods described there. For expression, COS-1 cells were transfected with cDNA inserted into expression vectors pMT2 (14), pcDNA3.1 (Invitrogen), or pcDNA6 (Invitrogen), using the calcium phosphate precipitation method (15). Microsomal vesicles containing the expressed SERCA construct were isolated by differential centrifugation (16). The concentration of expressed Ca^{2+}-ATPase was determined by measuring the maximum capacity for phosphorylation with [γ-^{32}P]ATP or $^{32}P_i$ ("active site concentration") (17).

Measurements of phosphorylation and dephosphorylation were generally carried out by manual mixing at 0 °C (17, 18). Transient state kinetics at 25 °C was analyzed using the Bio-Logic quench-flow module QFM-5 (Bio-Logic Science Instruments, Claix, France) with mixing protocols as previously described (19, 20). The determination of the phosphorylation level by acid quenching followed by acid SDS-polyacrylamide gel electrophoresis and quantification of the radioactivity associated with the Ca^{2+}-ATPase band was carried out using previously established procedures (17, 18, 20).

To determine a time course of phosphorylation or dephosphorylation, at least two independent series of kinetic experiments were carried out (see *n* values in Tables 1–3), with the earliest time points in duplicate in each series. Here *independent* means: carried out on different days, using enzyme preparations from different transfections. The complete set of data points collected (all shown in the graphs) was analyzed by nonlinear regression using the SigmaPlot program (SPSS, Inc.), and the extracted parameters with the S.E. values from the regression are reported in the tables. Monoexponential functions were fitted to the time courses of dephosphorylation, Ca^{2+} binding, and Ca^{2+} dissociation. The analysis of the Ca^{2+}-concentration dependence of phosphorylation was performed using the modified Hill equations given in the corresponding legends.

RESULTS

Design and Expression of the Chimeric and Mutant Ca^{2+}-ATPases—Nine wild type or modified Ca^{2+}-ATPase constructs were included in the present study (Fig. 1 and Table 1), designed with the purpose of elucidating the distinct influences of TM11 and LE on the partial reaction steps of the pump cycle (Scheme 1). The proteins were expressed in COS-1 cells to similar high levels, thus facilitating the study of the transient kinetics of the individual reactions. The results presented in the figures are summarized in Tables 2 and 3.

The wild types studied were the rabbit SERCA1a ("S1a"), human SERCA2a ("S2a"), and human SERCA2b ("S2b"). A group of loss of SERCA2b tail function mutants with alteration to the LE or TM11 of the SERCA2b tail were analyzed. "S2b-T1032*" is SERCA2b truncated just prior to Thr^{1032} by substituting the codon corresponding to Thr^{1032} with a STOP codon indicated by an asterisk (*), thereby deleting the entire 11-a-

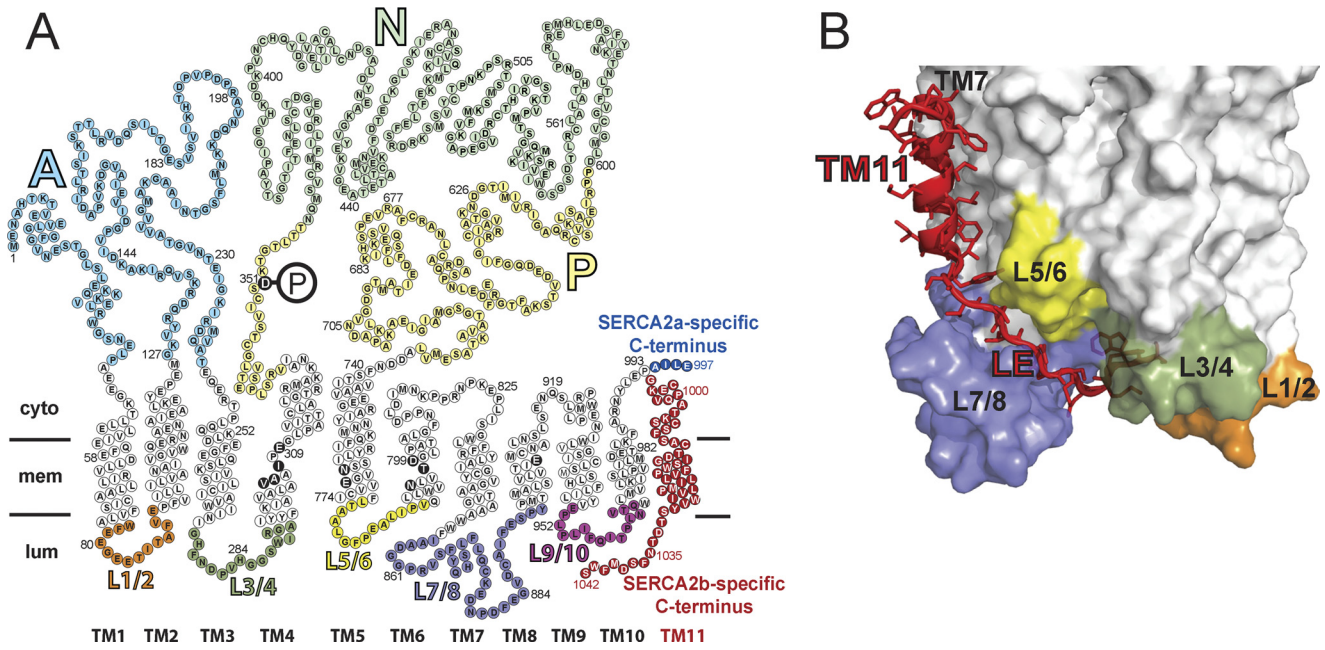

FIGURE 1. **Amino acid sequence and membrane topology of SERCA isoforms 2a and 2b, illustrating the difference in the C-terminal tail region (*A*), and three-dimensional model of the structural relationship of the extended C terminus of SERCA2b (*B*).** In *A*, each *circle* corresponds to an amino acid residue indicated by the *single-letter code inside the circle*. The phosphorylated aspartate (Asp^{351}) is indicated by *white lettering on black background* with a *large encircled P* attached. *TM1-TM11* denotes the transmembrane helices, of which TM11 is found only in SERCA2b. In the transmembrane helices, circles with *white lettering on black background* indicate the calcium binding residues. The unique C-terminal tail of SERCA2b is colored *red*, whereas the corresponding part of SERCA2a is shown in *blue*. SERCA2a and SERCA2b are identical in the first 993 amino acid residues. SERCA1a (994 residues, not shown) has a topology similar to SERCA2a with 84% amino acid identity. The SERCA2b-specific tail comprises in addition to TM11 also an 11-amino acid luminal extension (residues 1032–1042). The cytoplasmic domains *A*, *N*, and *P*, are indicated using different color codes, as are the luminal loops *L1/2*, *L3/4*, *L5/6*, *L7/8*, and *L9/10*. *B*, the C-terminal tail of SERCA2b modeled on a SERCA2a homology model derived from the crystal structure of SERCA1a in Ca_2E1 form (6). The modeled TM11 is in proximity to TM7 and TM10. As it descends from TM11 the luminal extension is in close contact with the luminal loop L7/8. The last four residues, MFWS, occupy a luminal docking site formed by luminal loops L1/2, L3/4, and L7/8 (6). The luminal loops are indicated by the same color code as in *A*.

TABLE 1
Overview of the chimeric and mutant Ca^{2+}-pump constructs studied

Construct	Description	Sequence of C-terminal amino acid residues
S1a	Rabbit SERCA1a wild type	^{988}ARNYLEG
S2a	Human SERCA2a wild type	^{987}ARNYLEPAILE
S2b	Human SERCA2b wild type	^{987}ARNYLEPGKECVQPATKSCSFSACTDG ISWPFVLLIMPLVIWVYSTDTNFSDMFWS
S2b-T1032*	S2b terminated before Thr^{1032}	^{987}ARNYLEPGKECVQPATKSCSFSACTDG ISWPFVLLIMPLVIWVYS
S2b-MFWS-AAAA	S2b with the C-terminal last four residues (MFWS) substituted with alanines	^{987}ARNYLEPGKECVQPATKSCSFSACTDG ISWPFVLLIMPLVIWVYSTDTNFSDAAAA
S1a2b	S1a with the C terminus of S2b	^{988}ARNYLEPGKECVQPATKSCSFSACTDG ISWPFVLLIMPLVIWVYSTDTNFSDMFWS
S1a2b-T1032*	S1a with the C terminus of S2b, terminated before Thr^{1032} [a]	^{988}ARNYLEPGKECVQPATKSCSFSACTDG ISWPFVLLIMPLVIWVYS
S1a2b-L7/8	S1a with the C terminus and the L7/8 luminal loop of S2b	Same as S1a2b
S1a-L7/8	S1a with the L7/8 luminal loop of S2b	Same as S1a

[a] Note that "1032" here refers to S2a/S2b numbering. Due to the presence of an extra amino acid in the nucleotide binding domain of S1a relative to S2a/S2b the S1a2b-T1032* chimera is actually one residue longer than S2b-T1032*.

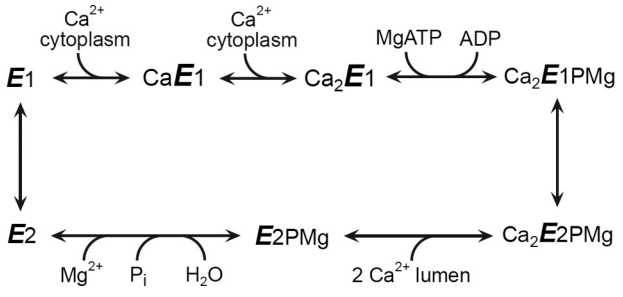

SCHEME 1. **Ca^{2+}-ATPase reaction cycle.** Major conformational changes and substrate binding and dissociation steps are shown.

mino acid LE of the SERCA2b tail (Fig. 1 and Table 1). In "S2b-MFWS-AAAA," the last four amino acid residues of the SERCA2b LE (^{1039}MFWS) are replaced by alanines.

A set of SERCA1a-2b chimeras were also studied, in which either the complete 49-amino acid C-terminal tail of SERCA2b was attached to SERCA1a ("S1a2b"), or only the part of the tail consisting of TM11 without the LE was attached to SERCA1a ("S1a2b-T1032*," *i.e.* S1a2b truncated as described for S2b-T1032*). The effect of simultaneously replacing the luminal loop connecting transmembrane helices TM7 and TM8 (L7/8) with the corresponding loop of SERCA2a/SERCA2b was also examined ("S1a2b-L7/8" with "S1a-L7/8" as reference), because the large L7/8 loop contains several amino acid differences between SERCA1 and SERCA2 isoforms and is likely to be in contact with the LE (Fig. 1*B*).

Rate of Ca^{2+} Dissociation Toward the Cytosolic Side—Ca^{2+} dissociation from Ca_2E1, *i.e.* toward the cytosolic side, was

TABLE 2

Rates of partial reactions

Rate constants ± S.E. values were obtained by nonlinear regression analysis of the data points shown in the figures. The number of independent experiments (performed with different enzyme preparations on different days) is indicated by *n*.

	Ca^{2+} dissociation toward the cytosol ($Ca_2E1 \rightarrow CaE1$)[a]	Conformational transition of the phosphoenzyme ($Ca_2E1P \rightarrow E2P$)[b]	Dephosphorylation of *E*2P ($E2P \rightarrow E2$)[c]	Conformational transition of the dephosphoenzyme ($E2 \rightarrow E1$)[d]
			$k\ (s^{-1})$	
S1a	2.49 ± 0.09 ($n = 5$)	0.109 ± 0.003 ($n = 11$)	0.099 ± 0.004 ($n = 8$)	1.00 ± 0.04 ($n = 11$)
S2a	4.23 ± 0.20 ($n = 2$)	0.087 ± 0.003 ($n = 2$)	0.064 ± 0.005 ($n = 2$)	0.60 ± 0.06 ($n = 3$)
S2b	0.77 ± 0.03 ($n = 2$)	0.049 ± 0.002 ($n = 5$)	0.030 ± 0.003 ($n = 3$)	0.26 ± 0.02 ($n = 3$)
S2b-T1032*	2.61 ± 0.13 ($n = 2$)	0.067 ± 0.004 ($n = 3$)	0.024 ± 0.002 ($n = 3$)	0.20 ± 0.01 ($n = 2$)
S2b-MFWS-AAAA	1.98 ± 0.09 ($n = 3$)	0.054 ± 0.001 ($n = 2$)	0.035 ± 0.004 ($n = 2$)	0.38 ± 0.03 ($n = 3$)
S1a2b	2.03 ± 0.14 ($n = 2$)	0.061 ± 0.004 ($n = 3$)	0.048 ± 0.003 ($n = 2$)	1.55 ± 0.17 ($n = 2$)
S1a2b-T1032*	1.99 ± 0.10 ($n = 2$)	0.048 ± 0.003 ($n = 2$)	0.067 ± 0.004 ($n = 2$)	1.84 ± 0.14 ($n = 3$)
S1a2b-L7/8	0.97 ± 0.04 ($n = 3$)	0.036 ± 0.003 ($n = 4$)	0.043 ± 0.003 ($n = 2$)	1.12 ± 0.10 ($n = 3$)
S1a-L7/8	1.42 ± 0.05 ($n = 2$)	0.093 ± 0.004 ($n = 2$)	0.101 ± 0.006 ($n = 2$)	0.54 ± 0.03 ($n = 3$)
Conclusion regarding involvement of LE and TM11	LE/MFWS is most critical, likely through interaction with L7/8.	The LE (but not the four C-terminal MFWS residues) and the TM11 are both important, the LE likely through interaction with L7/8.	LE (including MFWS) and L7/8 are not important. TM11 is critical. Interaction of TM11 with SERCA2 specific sequence element(s) is involved.	LE (including MFWS) is not important. TM11 is critical. Interaction of TM11 with SERCA2 specific sequence element(s) is involved.

[a] Data corresponding to Fig. 2.
[b] Data corresponding to Fig. 3.
[c] Data corresponding to Fig. 4.
[d] Data corresponding to Fig. 5.

TABLE 3

Apparent affinities for cytoplasmic and luminal Ca^{2+}

$K_{0.5}$ ± S.E. values were obtained by nonlinear regression analysis of data points. The number of independent experiments (performed with different enzyme preparations on different days) is indicated by *n*.

	Activation of phosphorylation from ATP by cytoplasmic Ca^{2+}, $K_{0.5}$	Activation of phosphorylation from P_i by luminal Ca^{2+}, $K_{0.5}$
	μM[a]	$m M$[b]
S1a	1.11 ± 0.02 ($n = 9$)	7.27 ± 0.14 ($n = 16$)
S2a	0.85 ± 0.04 ($n = 2$)	8.39 ± 0.89 ($n = 3$)
S2b	0.70 ± 0.04 ($n = 3$)	4.83 ± 0.44 ($n = 3$)
S2b-T1032*	0.75 ± 0.04 ($n = 2$)	5.97 ± 0.33 ($n = 3$)
S2b-MFWS-AAAA	0.88 ± 0.03 ($n = 4$)	5.37 ± 0.29 ($n = 3$)
S1a2b	0.59 ± 0.02 ($n = 3$)	4.11 ± 0.28 ($n = 3$)
S1a2b-T1032*	0.67 ± 0.02 ($n = 2$)	4.21 ± 0.22 ($n = 3$)
S1a2b-L7/8	0.43 ± 0.02 ($n = 2$)	3.24 ± 0.17 ($n = 3$)
S1a-L7/8	1.20 ± 0.04 ($n = 2$)	5.74 ± 0.19 ($n = 3$)

[a] Microsomes were pre-equilibrated at 0 °C in 40 mM MOPS/Tris (pH 7.0), 80 mM KCl, 5 mM $MgCl_2$, 1 mM EGTA, and various concentrations of $CaCl_2$ to obtain a series of free Ca^{2+} concentrations in the 0.1–100 μM range, followed by phosphorylation for 15 s at 0 °C with 5 μM [γ-^{32}P]ATP and subsequent acid quenching. The Hill equation, $EP = EP_{max} \cdot [Ca^{2+}]^h/(K_{0.5}{}^h + [Ca^{2+}]^h)$, was fitted to the data by nonlinear regression analysis (Hill coefficients (h) varying between 1.2 and 1.9).
[b] Data corresponding to Fig. 6.

examined in rapid kinetic measurements taking advantage of the requirement for occupancy of the two Ca^{2+} sites to allow phosphorylation from ATP. The mixing protocol is illustrated at the *top* of Fig. 2 (for a more detailed description of this method see Ref. 20). Upon addition of the Ca^{2+} chelator EGTA the ability to become phosphorylated by [γ-^{32}P]ATP disappears at a rate corresponding to the rate of Ca^{2+} dissociation (actually the rate corresponding to the Ca^{2+} ion dissociating first in the sequential mechanism, because both Ca^{2+} sites must be filled for phosphorylation to occur).

The Ca^{2+} dissociation was markedly slower for SERCA2b than for SERCA1a (3.2-fold) or SERCA2a (5.5-fold). Much of this effect seems attributable to the LE of the tail, as the truncation of SERCA2b at Thr^{1032} led to a marked 3.4-fold increase of the rate of Ca^{2+} dissociation (Fig. 2 and Table 2, S2b-T1032*). A conspicuous increase in the Ca^{2+} dissociation rate (2.6-fold) was also obtained by the less extensive modification in which only the last four amino acid residues (^{1039}MFWS) of the SERCA2b LE were replaced by alanines (Fig. 2 and Table 2, S2b-MFWS-AAAA), implying that these last four amino acids are critical for Ca^{2+} dissociation. TM11 may also be of some minor importance in determining the slow Ca^{2+} dissociation of SERCA2b, because the removal of TM11 resulted in a 1.6-fold increase of the Ca^{2+} dissociation rate (compare SERCA2a with S2b-T1032*). Similar conclusions can be drawn from the gain of function approach. Hence, although addition of the SERCA2b tail to SERCA1a, with or without the LE (S1a2b and S1a2b-T1032*, respectively) had only a slight effect on the rate of Ca^{2+} dissociation (1.2-fold reduction), suggesting a modest role for TM11, combining the addition of the SERCA2b tail to SERCA1a with substituting the L7/8 loop of SERCA1a with that of SERCA2b (S1a2b-L7/8) led to a marked 2.6-fold reduction of the rate of Ca^{2+} dissociation (Fig. 2). This yields a rate not far from that of wild type SERCA2b (3.2-fold lower than that of wild type SERCA1a), indicating that the L7/8 loop of SERCA2b is required for the tail, in particular LE, to fully exert its effect on Ca^{2+} dissociation. A control experiment in which the L7/8 loop of SERCA1a was replaced with that of SERCA2b in the absence of the SERCA2b tail (S1a-L7/8), to reveal any effect of the L7/8 substitution *per se*, showed a less pronounced reduction of the Ca^{2+} dissociation rate by only 1.8-fold (Fig. 2 and Table 2).

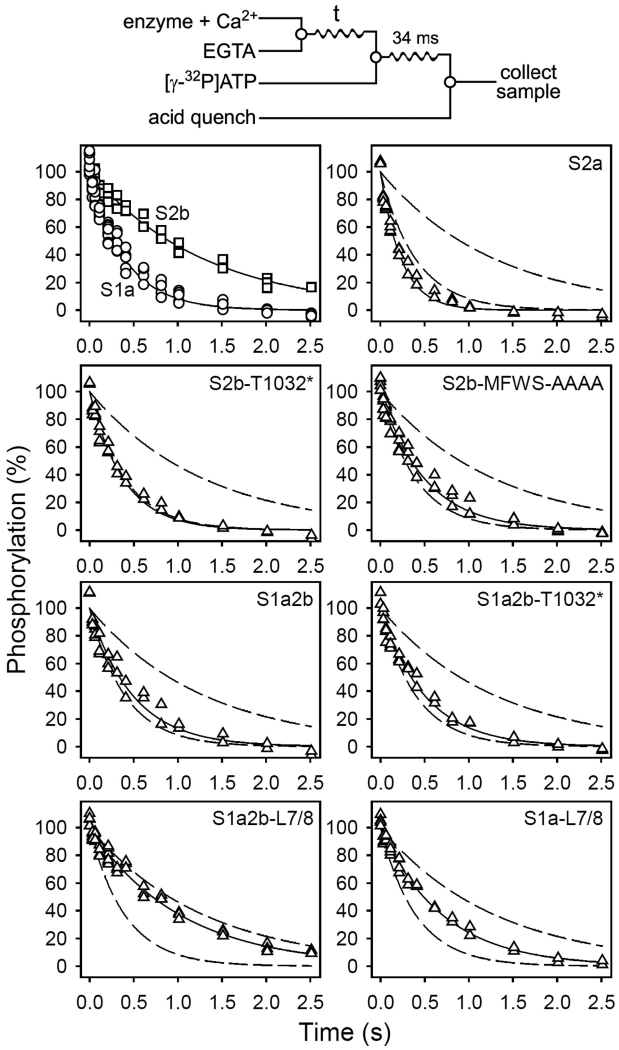

FIGURE 2. **Kinetics of the dissociation of Ca^{2+} at the cytoplasmically facing sites.** Quench-flow experiments were carried out by the mixing protocol illustrated by the *diagram above the panels* using a QFM-5 module at 25 °C. The microsomal enzyme, preincubated in 40 mM MES/Tris (pH 6.0), 80 mM KCl, 5 mM $MgCl_2$, and 100 μM $CaCl_2$ (to accumulate Ca_2E1), was mixed with an equal volume of 40 mM MES/Tris (pH 6.0), 80 mM KCl, 5 mM $MgCl_2$, and 4 mM EGTA, to initiate Ca^{2+} dissociation. At the indicated time intervals the amount of phosphorylatable Ca_2E1 remaining was determined by adding the double volume of 40 mM MES/Tris (pH 6.0), 80 mM KCl, 5 mM $MgCl_2$, 2 mM EGTA, and 10 μM [γ-^{32}P]ATP, followed by acid quenching 34 ms later. To obtain the point corresponding to zero time (in each case taken as 100%), 4 mM EGTA was replaced by 100 μM $CaCl_2$. All data points are shown. The *lines* show the best nonlinear regression fits of a monoexponential decay function, giving the rate constants listed in Table 2. The *broken lines* represent the curves corresponding to wild type SERCA1a and SERCA2b from the *upper left panel*.

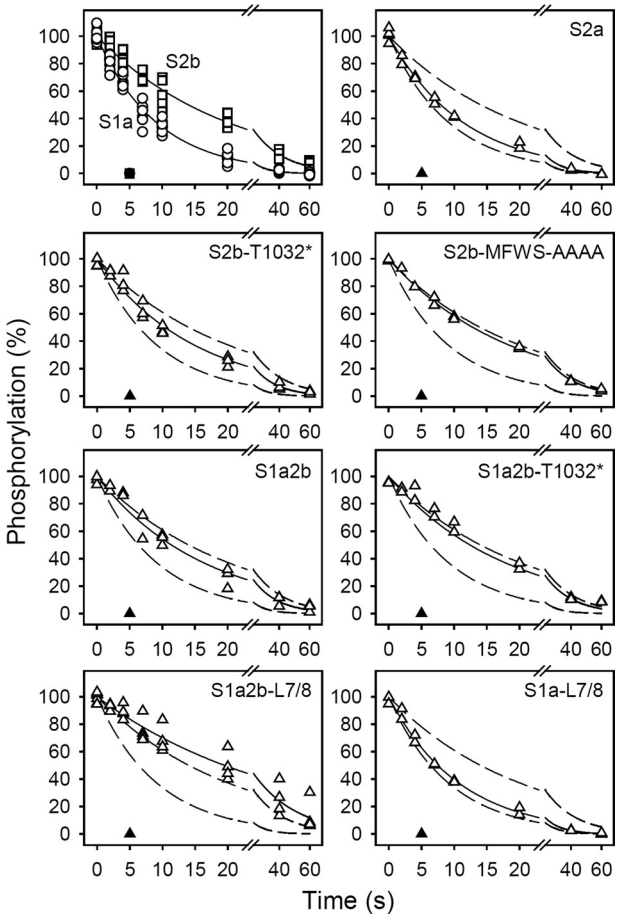

FIGURE 3. **Kinetics of the $Ca_2E1P \rightarrow E2P$ transition.** The microsomal enzyme was phosphorylated by incubation for 15 s at 0 °C in 40 mM MOPS/Tris (pH 7.0), 80 mM KCl, 5 mM $MgCl_2$, 1 mM EGTA, 0.955 mM $CaCl_2$ (giving a free Ca^{2+} concentration of 10 μM during phosphorylation), 2 μM calcium ionophore A23187, and 5 μM [γ-^{32}P]ATP. Dephosphorylation was then studied at 0 °C by addition of excess EGTA (to remove Ca^{2+} and, thus, terminate phosphorylation) followed by acid quenching at the indicated time intervals (*open symbols*). All data points are shown. The *lines* show the best nonlinear regression fits of a monoexponential decay function, giving the rate constants listed in Table 2. The *closed symbols* represent similar experiments in which 1 mM ADP was added together with the EGTA chase medium. In each case, the 100% value corresponds to the steady-state level of phosphoenzyme present just prior to the initiation of dephosphorylation. The *broken lines* represent the curves corresponding to wild type SERCA1a and SERCA2b from the *upper left panel*.

These findings are supportive of a model where the LE docks near L7/8 (Fig. 1*B*).

Rate of $Ca_2E1P \rightarrow E2P$—To study this conformational transition, the enzyme was first phosphorylated by [γ-^{32}P]ATP, and the phosphoenzyme was then chased at 0 °C by addition of excess EGTA (to terminate phosphorylation by removal of Ca^{2+}) with or without 1 mM ADP (Fig. 3). As shown by the *closed symbols* in Fig. 3, the accumulated phosphoenzyme disappeared rapidly in the presence of ADP for both the wild type pumps and the mutants, indicating that the major phosphoenzyme form accumulated is ADP-sensitive Ca_2E1P, *i.e.* for all constructs the transition of this form to the ADP-insensitive *E*2P phosphoenzyme intermediate is the rate-limiting step in the $Ca_2E1P \rightarrow E2P \rightarrow E2$ reaction sequence under the specific conditions applied here. Hence, the rate of dephosphorylation observed when phosphorylation was terminated by adding EGTA in the absence of ADP (*open symbols* in Fig. 3) reflects the $Ca_2E1P \rightarrow E2P$ reaction step.

The data in Fig. 3 show that SERCA2b undergoes the $Ca_2E1P \rightarrow E2P$ reaction step ~2-fold slower than SERCA1a and SERCA2a (see also Table 2), a characteristic that contributes to determine the high apparent Ca^{2+} affinity of SERCA2b relative to SERCA1a and SERCA2a, because less Ca^{2+} is required for a certain amount of phosphoenzyme to accumulate, when $Ca_2E1P \rightarrow E2P$ is slow (10, 13). Truncation of the SERCA2b LE increased the $Ca_2E1P \rightarrow E2P$ rate 1.4-fold (Fig. 3 and Table 2, S2b-T1032*), indicating a role of the LE in determining the low $Ca_2E1P \rightarrow E2P$ rate in wild type SERCA2b. Adding the

SERCA2b C-terminal tail to SERCA1a, with (S1a2b) or even without (S1a2b-T1032*) the LE, reduced the rate of $Ca_2E1P \rightarrow E2P$ to a level close to that of SERCA2b, thus indicating that TM11 is important as well. Simultaneous addition of the entire SERCA2b C-terminal tail to SERCA1a and substitution of the L7/8 loop (S1a2b-L7/8) further strengthened the effect, whereas substitution of the L7/8 loop of SERCA1a with that of SERCA2b in the absence of the SERCA2b tail (S1a-L7/8) had little effect on the rate of $Ca_2E1P \rightarrow E2P$. Hence, both the LE and the TM11 contribute to the low rate of the $Ca_2E1P \rightarrow E2P$ transition in wild type SERCA2b, and the effect depends on the L7/8 loop, likely because it interacts with the LE. However, the last four residues of the LE are not much involved in this effect, because their replacement by alanines (S2b-MFWS-AAAA) had almost no impact, if any, on the rate of $Ca_2E1P \rightarrow E2P$.

Rate of E2P → E2 Dephosphorylation—The dephosphorylation of the *E*2P phosphoenzyme was examined by first phosphorylating the Ca^{2+}-deprived enzyme by $^{32}P_i$ in the backward direction of the normal reaction cycle to accumulate *E*2P (*cf.* Scheme 1), and then chasing the *E*2P phosphoenzyme by dilution into a dephosphorylation buffer containing nonradioactive P_i at pH 7 and only little (10 mM) K^+ to ensure a relatively slow dephosphorylation thereby allowing a very accurate measurement, *cf.* Ref. 21).

As seen in Fig. 4 and Table 2, *E*2P dephosphorylation was markedly slower for SERCA2b than for SERCA1a (3-fold) and SERCA2a (1.5-fold). Neither substitution of the last four residues of SERCA2b by alanines (S2b-MFWS-AAAA) nor truncation of the entire SERCA2b LE (S2b-T1032*) had any impact on *E*2P dephosphorylation. A ~2-fold slowing of *E*2P dephosphorylation was seen upon adding the C-terminal tail to SERCA1a, but this effect was not dependent on simultaneous substitution of the L7/8 loop (compare S1a2b with S1a2b-L7/8 in Fig. 4 and Table 2). These findings indicate that TM11, but not the LE, is critical for the slower *E*2P dephosphorylation in SERCA2b. It is also noteworthy that the efficiency of TM11 in slowing the dephosphorylation is less when added to SERCA1a as compared with the SERCA2 environment (compare S1a2b with S2b and S1a2b-T1032* with S2b-T1032* in Fig. 4 and Table 2). This suggests that direct or indirect interaction of the TM11 with SERCA2-specific sequence element(s) elsewhere in the protein is involved.

Rate of E2 → E1—Another possible determinant of the apparent affinity for Ca^{2+} activation of the overall reaction is the rate of the *E*2 → *E*1 transition of the dephosphoenzyme, *i.e.* the step immediately preceding Ca^{2+} binding at the cytoplasmically facing high affinity Ca^{2+} sites. Fig. 5 shows the kinetics of the *E*2 → *E*1 → Ca_2E1 reaction sequence under conditions where the *E*2 → *E*1 transition is rate-limiting because of the low pH (pH 6) (22). It is apparent from Fig. 5 and Table 2 that the SERCA2b tail slows the rate of *E*2 → *E*1, SERCA2b displaying 2.3-fold lower rate than SERCA2a and a 3.8-fold lower rate than SERCA1a. Because the rate of the *E*2 → *E*1 transition influences the amount of *E*1 available for Ca^{2+} binding at steady-state, a slow *E*2 → *E*1 transition should in principle tend to reduce the apparent Ca^{2+} affinity observed in steady-state measurements of the overall ATPase reaction, however, because the slow phosphoenzyme processing as well as the slow Ca^{2+} dissociation exert the opposite effect, tending to increase the apparent Ca^{2+} affinity, the net result is that a high apparent Ca^{2+} affinity prevails in SERCA2b relative to the other isoforms.

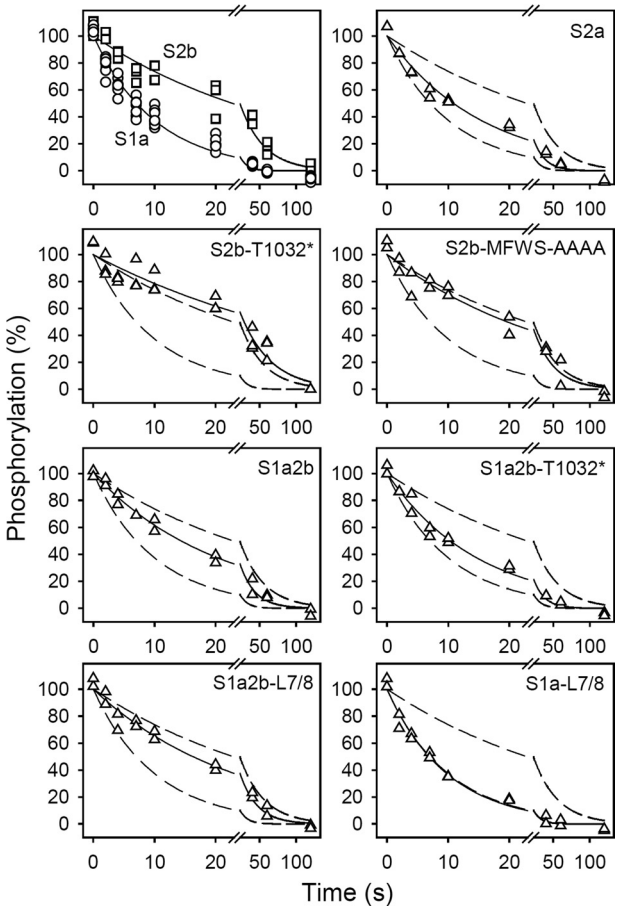

FIGURE 4. **Kinetics of *E*2P dephosphorylation.** The microsomal enzyme was phosphorylated for 10 min at 25 °C in 100 mM MES/Tris (pH 6.0), 10 mM $MgCl_2$, 2 mM EGTA, 30% (v/v) dimethyl sulfoxide (the organic solvent ensuring maximal amount of phosphoenzyme), and 0.5 mM $^{32}P_i$. Dephosphorylation was then studied at 0 °C by a 19-fold dilution of pre-chilled phosphorylated microsomes into ice-cold medium containing 40 mM MOPS/Tris (pH 7.0), 10 mM KCl, 2 mM $MgCl_2$, 2 mM EGTA, and 0.5 mM nonradioactive P_i, followed by acid quenching at the indicated time intervals. All data points are shown. The *lines* show the best nonlinear regression fits of a monoexponential decay function, giving the rate constants listed in Table 2. In each case, the 100% value corresponds to the level of phosphoenzyme present just prior to the initiation of dephosphorylation. The *broken lines* represent the curves corresponding to wild type SERCA1a and SERCA2b from the *upper left panel*.

Truncation of the SERCA2b LE (S2b-T1032*) did not increase the *E*2 → *E*1 rate, indicating that TM11 is responsible for the low rate in SERCA2b. The addition of the SERCA2b tail to SERCA1a without or with concomitant substitution of the L7/8 loop with that of SERCA2b (S1a2b and S1a2b-L7/8, respectively) did not reduce the rate of *E*2 → *E*1 relative to that of the SERCA1a wild type. Hence, SERCA2-specific element(s) elsewhere in the protein must be involved in causing the slow *E*2 → *E*1 imposed by TM11, in line with the findings in relationship to *E*2P dephosphorylation. However, because the mere substitution of the L7/8 loop in SERCA1a with that of SERCA2 (S1a-L7/8) resulted in a rate of *E*2 → *E*1 somewhat slower than that of SERCA1a and similar to that of SERCA2a, a SERCA2-specific element of the L7/8 loop might also in some way contribute to the slowing of *E*2 → *E*1.

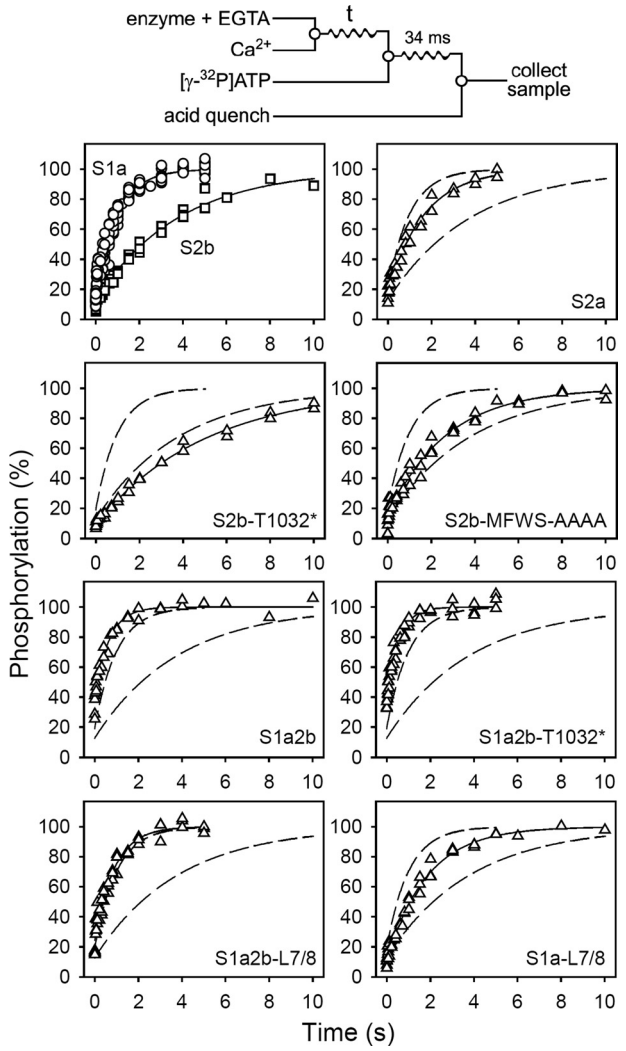

FIGURE 5. **Kinetics of the *E*2 → *E*1 transition.** Quench-flow experiments were carried out by the mixing protocol illustrated in the *diagram above the panels* using a QFM-5 module at 25 °C. The microsomal enzyme, preincubated in 40 mM MES/Tris (pH 6.0), 80 mM KCl, and 2 mM EGTA (to accumulate *E*2), was mixed with an equal volume of 40 mM MES/Tris (pH 6.0), 80 mM KCl, and 2.2 mM $CaCl_2$. At the indicated time intervals, the amount of phosphorylatable Ca_2E1 was determined by adding the double volume of 40 mM MES/Tris (pH 6.0), 80 mM KCl, 10 mM $MgCl_2$, 1 mM EGTA, 10 μM [γ-^{32}P]ATP, and 1.1 mM $CaCl_2$, followed by acid quenching 34 ms later. To obtain the point corresponding to zero time, the enzyme was preincubated in 40 mM MES/Tris (pH 6.0), 80 mM KCl, and 2 mM EGTA and mixed with an equal volume of 40 mM MES/Tris (pH 6.0), 80 mM KCl, 10 mM $MgCl_2$, 10 μM [γ-^{32}P]ATP, and 2.2 mM $CaCl_2$, followed by acid quenching 34 ms later. All data points are shown. The *lines* represent the best nonlinear regression fits of a monoexponential "rise to max" function with an initial offset, giving the rate constants listed in Table 2. In each case, the phosphorylation level at infinite time extracted from the fit was taken as 100%. The *broken lines* represent the curves corresponding to wild type SERCA1a and SERCA2b from the *upper left panel*.

Comparison of Apparent Ca^{2+} Affinities at Cytoplasmic and Luminal Sites—The Ca^{2+} concentration dependence of steady-state phosphorylation of Ca_2E1 from [γ-^{32}P]ATP was studied to evaluate the combined effects of the changes to the partial reaction steps on apparent Ca^{2+} affinity of the cytoplasmically facing sites (Table 3, first column). A higher apparent Ca^{2+} affinity is seen for SERCA2b, relative to SERCA1a and SERCA2a. The apparent Ca^{2+} affinity of SERCA2b was lowered by manipulations to the tail and increased by addition of the SERCA2b tail to SERCA1a, in particular in combination with the L7/8 loop substitution. Both the LE and TM11 appear to contribute. These results are in good agreement with our findings for the rate constants of the individual partial reactions and with previous analysis of the overall reaction by measurement of the Ca^{2+} dependence of steady-state ATPase activity (6).

The effect of the entire SERCA2b tail and its separate LE and TM11 parts on the apparent Ca^{2+} affinity of the luminally facing low-affinity Ca^{2+} sites has not previously been determined. To this end, we studied the dependence of phosphorylation of *E*2 from inorganic phosphate on luminal Ca^{2+} (*cf.* Scheme 1 and Refs. 23–25). Microsomal vesicles containing wild type or mutant Ca^{2+} pumps were loaded passively with various Ca^{2+} concentrations overnight and then diluted into a medium containing $^{32}P_i$ and EGTA to observe the phosphorylation from $^{32}P_i$ occurring in the absence of free Ca^{2+} in the medium outside the vesicles.

The data obtained are shown in Fig. 6 and Table 3, second column. Increasing the luminal Ca^{2+} concentration stimulated the phosphorylation from $^{32}P_i$ with apparent Ca^{2+} affinities of the SERCA1a, SERCA2a, and SERCA2b wild type pumps corresponding to $K_{0.5}$ values of 7.3, 8.4, and 4.8 mM Ca^{2+}, respectively, thus indicating that the apparent Ca^{2+} affinity is highest for SERCA2b, not only on the cytoplasmic side, but on the luminal side as well.

The manipulations to the SERCA2b LE (S2b-T1032* and S2b-MFWS-AAAA) slightly increased the $K_{0.5}$ for the luminal Ca^{2+} activation of phosphorylation from $^{32}P_i$ relative to the SERCA2b wild type. Adding the SERCA2b tail to SERCA1a with (S1a2b) or without (S1a2b-T1032*) the LE reduced the $K_{0.5}$ for luminal Ca^{2+} to a value similar to that of SERCA2b. Replacement of the L7/8 loop of SERCA1a with that of SERCA2 (S1a-L7/8) reduced the $K_{0.5}$ for Ca^{2+}, however, the simultaneous substitution of the L7/8 loop and addition of the SERCA2b tail to SERCA1a (S1a2b-L7/8) resulted in the lowest $K_{0.5}$ for Ca^{2+} of all constructs. Collectively, these results suggest that TM11 is the main determinant of the higher apparent luminal Ca^{2+} affinity of SERCA2b relative to the other isoforms, but the LE also contributes to some extent via its interaction with the L7/8 loop. Despite the more than 1000-fold difference in the actual affinities for cytoplasmic and luminal Ca^{2+}, there is a remarkable correlation between the apparent affinities for Ca^{2+} on the two sides of the membrane, as illustrated in Fig. 7 by the plot of the $K_{0.5}$ values observed for cytoplasmic Ca^{2+} against the $K_{0.5}$ values observed for luminal Ca^{2+}.

DISCUSSION

The SERCA2b tail changes the kinetics of the Ca^{2+} pump at various partial reaction steps, inducing (i) a slower Ca^{2+} dissociation from the high-affinity sites in Ca_2E1 toward the cytosol, (ii) a slower $Ca_2E1P \rightarrow E2P$ transition, (iii) slower *E*2P dephosphorylation, and (iv) a reduced rate of $E2 \rightarrow E1$. The present kinetic analysis of the partial reaction steps of mutants and chimeric constructs has demonstrated that TM11 and the LE differentially affect these steps that determine the high apparent Ca^{2+} affinity and low maximal turnover rate of SERCA2b. The major conclusions are indicated below the rate constants in Table 2.

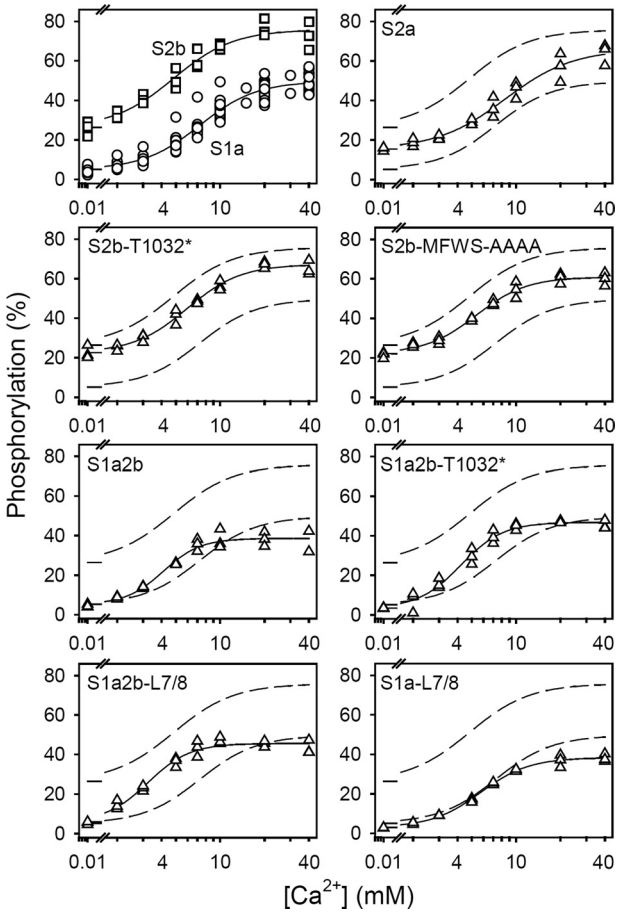

FIGURE 6. **Dependence of phosphorylation from $^{32}P_i$ on the luminal Ca^{2+} concentration.** Microsomal vesicles were loaded with Ca^{2+} in the lumen by incubation overnight (~18 h) on ice in 150 mM MOPS/Tris (pH 7.0), 125 mM sucrose, 75 mM KCl, and the indicated Ca^{2+} concentration added as $CaCl_2$. The phosphorylation was then determined at 25 °C by a 50-fold dilution of the Ca^{2+}-loaded vesicles into a phosphorylation medium containing 150 mM MOPS/Tris (pH 7.0), 125 mM sucrose, 77 mM KCl, 10 mM EGTA (removing Ca^{2+} from the medium outside the vesicles), and 0.5 mM $^{32}P_i$, followed by acid quenching 1 min later. The *ordinate* shows the results as percentage of the maximal phosphorylation level obtained by phosphorylation from $^{32}P_i$ under optimal conditions for *E*2P formation in the presence of dimethyl sulfoxide, as described in the legend to Fig. 4. All data points are shown. The *lines* show the best nonlinear regression fits of a modified Hill equation $EP = EP_{min} + (EP_{\infty} - EP_{min}) \cdot [Ca^{2+}]^n/(K_{0.5}{}^n + [Ca^{2+}]^n)$, with EP_{min} accounting for the basic phosphorylation level in the absence of a Ca^{2+} gradient and EP_{∞} representing the extrapolated phosphorylation level at infinite intravesicular Ca^{2+}. The $K_{0.5}$ values obtained are listed in Table 3. The *broken lines* represent the curves corresponding to wild type SERCA1a and SERCA2b from the *upper left panel*.

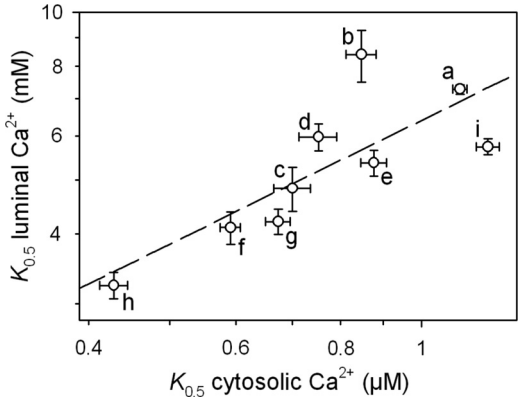

FIGURE 7. **Correlation between the apparent Ca^{2+} affinities of cytoplasmically and luminally facing sites.** The $K_{0.5}$ values for Ca^{2+} activation of phosphorylation from the cytoplasmic and luminal side (data from Table 3) are represented by the *abscissa* and *ordinate*, respectively, on a logarithmic scale. The labeling is as follows: *a,* S1a; *b*, S2a; *c*, S2b; *d*, S2b-T1032*; *e*, S2b-MFWS-AAAA; *f*, S1a2b; *g*, S1a2b-T1032*; *h*, S1a2b-L7/8; *i*, S1a-L7/8.

Role of the LE—The LE (particularly the last four residues, MFWS) was shown here to be critical to the slow Ca^{2+} dissociation from Ca_2E1 toward the cytosolic side in SERCA2b. The gain of SERCA2b tail function with respect to the slow Ca^{2+} dissociation from Ca_2E1 observed upon addition of the SERCA2b tail to SERCA1a depends on simultaneous substitution of the L7/8 loop with that of SERCA2, thus suggesting that the LE interacts with L7/8 to stabilize the Ca^{2+} bound Ca_2E1 state. Such a scenario appears realistic from a structural point of view, if the LE docks between the luminal L3/4 and L7/8 loops at a site available only in the Ca_2E1 state and not in *E*2 as proposed by the model in Fig. 1*B* (6), because M4, which is connected to L3/4, plays a central role in the function of the Ca^{2+} sites (26, 27). The structural change underlying the stabilizing effect of the LE on Ca_2E1 might be related to the change in the proteinase K cleavage pattern observed upon addition of synthetic LE peptide to SERCA2a, showing the appearance of a 90-kDa cleavage product (6).

The LE and L7/8 are also important for the low rate of the Ca^{2+} translocating conformational change $Ca_2E1P \rightarrow E2P$ in SERCA2b, which likewise may owe to a stabilization of a Ca^{2+} bound form, in this case the Ca_2E1P phosphoenzyme, which has Ca^{2+} in the occluded state. However, it is noteworthy that the data (*cf.* Table 2) shows that the interaction of the LE in Ca_2E1P involves the four C-terminal MFWS residues to a much lesser extent than in Ca_2E1, thus indicating that the occlusion of the Ca^{2+} ions affects the docking of the C terminus.

Role of TM11—Although the TM11 seems to affect all the partial reaction steps studied to some extent, TM11 is most critical to the *E*2P dephosphorylation step, $E2P \rightarrow E2$, and the conformational transition of the dephosphoenzyme, $E2 \rightarrow E1$. The latter two steps are not at all dependent on the LE, and in contrast to the $Ca_2E1P \rightarrow E2P$ transformation, the $E2P \rightarrow E2$ and $E2 \rightarrow E1$ steps are highly dependent on the presence of TM11 in a SERCA2 environment. This applies with or without the LE present and irrespective of simultaneous exchange of L7/8, thus indicating that interaction of the TM11 with a SERCA2-specific sequence element(s) elsewhere in the structure is critical in the *E*2/*E*2P states.

Exactly how TM11 exerts the functional effects and which interaction partners are involved remain unclear in the absence of rigorous structural information about the relationship of the SERCA2b tail. Modeling based on the SERCA1a crystal structure (Fig. 1*B*) suggests that in addition to TM10, TM7 also might be an interaction partner of TM11 in SERCA2b, and both of these transmembrane helices contain residues that are not conserved between SERCA2 and SERCA1 isoforms (7). Moreover, SERCA2-specific sequence element(s) in cytoplasmic segments might play an indirect role by influencing the positioning of transmembrane segment(s) that interact with TM11. It is possible that in SERCA2b, TM11, like the β-subunit of Na^+,K^+-ATPase, impinges on TM7 and causes this helix to kink (7). The observation of such interaction in Na^+,K^+-

ATPase relates to the K^+-bound *E*2 conformation, and a role in determining K^+ selectivity has been suggested (28). Along the same line, interaction between TM11 and TM7 specific for *E*2/*E*2P states (*i.e.* the states corresponding to those binding K^+ in Na^+,K^+-ATPase) might be part of a mechanism slowing the *E*2P → *E*2 and *E*2 → *E*1 reactions in SERCA2b.

Conclusions—The present data indicate that docking of the LE near L7/8 preferentially stabilizes Ca_2E1 and Ca_2E1P, thus slowing Ca^{2+} dissociation from SERCA2b and thereby increasing the "true" (intrinsic) Ca^{2+} affinity, whereas functional interaction of the TM11 with a SERCA2-specific sequence element(s) elsewhere in the structure occurs particularly in the Ca^{2+}-free *E*2/*E*2P states, slowing *E*2P → *E*2 and *E*2 → *E*1 transitions and thereby reducing the maximal turnover rate of SERCA2b and increasing the apparent Ca^{2+} affinity by an indirect mechanism quite different from that of the LE.

The stabilization of Ca_2E1P as well as the slow *E*2P → *E*2 and *E*2 → *E*1 transitions favor the phosphorylation of *E*2 by P_i promoted by luminal Ca^{2+} and the subsequent accumulation of Ca_2E1P formed backwards from *E*2P. Collectively these effects therefore also explain that not only the apparent affinity for Ca^{2+} binding from the cytoplasmic side is enhanced in SERCA2b relative to the other isoforms, but in addition the apparent affinity for Ca^{2+} binding from the luminal side is affected in a similar manner. This previously unrecognized property of SERCA2b likely limits the capacity for Ca^{2+} storage by SERCA2b, because the luminal Ca^{2+} concentration at which "back inhibition" of the pump occurs is lower for SERCA2b than for other SERCA isoforms. Together with the lower maximal pump activity the limited storage capacity of SERCA2b may constitute an important reason why the housekeeping SERCA2b is replaced by/supplemented with SERCA1a, SERCA2a, or SERCA3 in cells that cope with large amounts of Ca^{2+}.

Acknowledgments—We thank Lene Jacobsen and Karin Kracht, Department of Biomedicine, Aarhus University, for expert technical assistance.

REFERENCES

1. Toyoshima, C. (2009) How Ca^{2+}-ATPase pumps ions across the sarcoplasmic reticulum membrane. *Biochim. Biophys. Acta* **1793,** 941–946
2. Møller, J. V., Olesen, C., Winther, A. M., and Nissen, P. (2010) The sarcoplasmic Ca^{2+}-ATPase. Design of a perfect chemi-osmotic pump. *Q. Rev. Biophys.* **43,** 501–566
3. Lytton, J., and MacLennan, D. H. (1988) Molecular cloning of cDNAs from human kidney coding for two alternatively spliced products of the cardiac Ca^{2+}-ATPase gene. *J. Biol. Chem.* **263,** 15024–15031
4. Verboomen, H., Wuytack, F., De Smedt, H., Himpens, B., and Casteels, R. (1992) Functional difference between SERCA2a and SERCA2b Ca^{2+} pumps and their modulation by phospholamban. *Biochem. J.* **286,** 591–595
5. Bayle, D., Weeks, D., and Sachs, G. (1995) The membrane topology of the rat sarcoplasmic and endoplasmic reticulum calcium ATPases by *in vitro* translation scanning. *J. Biol. Chem.* **270,** 25678–25684
6. Vandecaetsbeek, I., Trekels, M., De Maeyer, M., Ceulemans, H., Lescrinier, E., Raeymaekers, L., Wuytack, F., and Vangheluwe, P. (2009) Structural basis for the high Ca^{2+} affinity of the ubiquitous SERCA2b Ca^{2+} pump. *Proc. Natl. Acad. Sci. U.S.A.* **106,** 18533–18538
7. Gorski, P. A., Trieber, C. A., Larivière, E., Schuermans, M., Wuytack, F., Young, H. S., and Vangheluwe, P. (2012) Transmembrane helix 11 is a genuine regulator of the endoplasmic reticulum Ca^{2+} pump and acts as a functional parallel of β-subunit on α-Na^+,K^+-ATPase. *J. Biol. Chem.* **287,** 19876–19885
8. Verboomen, H., Wuytack, F., Van den Bosch, L., Mertens, L., and Casteels, R. (1994) The functional importance of the extreme C-terminal tail in the gene 2 organellar Ca^{2+}-transport ATPase (SERCA2a/b). *Biochem. J.* **303,** 979–984
9. Dode, L., Vilsen, B., Van Baelen, K., Wuytack, F., Clausen, J. D., and Andersen, J. P. (2002) Dissection of the functional differences between sarco(endo)plasmic reticulum Ca^{2+}-ATPase (SERCA) 1 and 3 isoforms by steady-state and transient kinetic analyses. *J. Biol. Chem.* **277,** 45579–45591
10. Dode, L., Andersen, J. P., Leslie, N., Dhitavat, J., Vilsen, B., and Hovnanian, A. (2003) Dissection of the functional differences between sarco(endo)plasmic reticulum Ca^{2+}-ATPase (SERCA) 1 and 2 isoforms and characterization of Darier disease (SERCA2) mutants by steady-state and transient kinetic analyses. *J. Biol. Chem.* **278,** 47877–47889
11. Bobe, R., Bredoux, R., Corvazier, E., Andersen, J. P., Clausen, J. D., Dode, L., Kovács, T., and Enouf, J. (2004) Identification, expression, function, and localization of a novel (sixth) isoform of the human sarco/endoplasmic reticulum Ca^{2+}-ATPase 3 gene. *J. Biol. Chem.* **279,** 24297–24306
12. Dally, S., Bredoux, R., Corvazier, E., Andersen, J. P., Clausen, J. D., Dode, L., Fanchaouy, M., Gelebart, P., Monceau, V., Del Monte, F., Gwathmey, J. K., Hajjar, R., Chaabane, C., Bobe, R., Raies, A., and Enouf, J. (2006) Ca^{2+}-ATPases in non-failing and failing heart. Evidence for a novel cardiac sarco/endoplasmic reticulum Ca^{2+}-ATPase 2 isoform (SERCA2c). *Biochem. J.* **395,** 249–258
13. Andersen, J. P., Sørensen, T. L., Povlsen, K., and Vilsen, B. (2001) Importance of transmembrane segment M3 of the sarcoplasmic reticulum Ca^{2+}-ATPase for control of the gateway to the Ca^{2+} sites. *J. Biol. Chem.* **276,** 23312–23321
14. Kaufman, R. J., Davies, M. V., Pathak, V. K., and Hershey, J. W. (1989) The phosphorylation state of eucaryotic initiation factor 2 alters translational efficiency of specific mRNAs. *Mol. Cell. Biol.* **9,** 946–958
15. Chen, C., and Okayama, H. (1987) High-efficiency transformation of mammalian cells by plasmid DNA. *Mol. Cell. Biol.* **7,** 2745–2752
16. Maruyama, K., and MacLennan, D. H. (1988) Mutation of aspartic acid 351, lysine 352, and lysine 515 alters the Ca^{2+} transport activity of the Ca^{2+}-ATPase expressed in COS-1 cells. *Proc. Natl. Acad. Sci. U.S.A.* **85,** 3314–3318
17. Sørensen, T., Vilsen, B., and Andersen, J. P. (1997) Mutation Lys-758 → Ile of the sarcoplasmic reticulum Ca^{2+}-ATPase enhances dephosphorylation of E2P and inhibits the *E*2 to $E1Ca_2$ transition. *J. Biol. Chem.* **272,** 30244–30253
18. Vilsen, B., Andersen, J. P., Clarke, D. M., and MacLennan, D. H. (1989) Functional consequences of proline mutations in the cytoplasmic and transmembrane sectors of the Ca^{2+}-ATPase of sarcoplasmic reticulum. *J. Biol. Chem.* **264,** 21024–21030
19. Sørensen, T. L., Dupont, Y., Vilsen, B., and Andersen, J. P. (2000) Fast kinetic analysis of conformational changes in mutants of the Ca^{2+}-ATPase of sarcoplasmic reticulum. *J. Biol. Chem.* **275,** 5400–5408
20. Clausen, J. D., and Andersen, J. P. (2004) Functional consequences of alterations to Thr-247, Pro-248, Glu-340, Asp-813, Arg-819, and Arg-822 at the interfaces between domain P, M3, and L6–7 of sarcoplasmic reticulum Ca^{2+}-ATPase. Roles in Ca^{2+} interaction and phosphoenzyme processing. *J. Biol. Chem.* **279,** 54426–54437
21. Sørensen, T. L., Clausen, J. D., Jensen, A. M., Vilsen, B., Møller, J. V., Andersen, J. P., and Nissen, P. (2004) Localization of a K^+-binding site involved in dephosphorylation of the sarcoplasmic reticulum Ca^{2+}-ATPase. *J. Biol. Chem.* **279,** 46355–46358
22. Forge, V., Mintz, E., and Guillain, F. (1993) Ca^{2+} binding to sarcoplasmic reticulum ATPase revisited. II. Equilibrium and kinetic evidence for a two-route mechanism. *J. Biol. Chem.* **268,** 10961–10968
23. Marchand, A., Winther, A. M., Holm, P. J., Olesen, C., Montigny, C., Arnou, B., Champeil, P., Clausen, J. D., Vilsen, B., Andersen, J. P., Nissen, P., Jaxel, C., Møller, J. V., and le Maire, M. (2008) Crystal structure of D351A and P312A mutant forms of the mammalian sarcoplasmic reticu-

lum Ca^{2+}-ATPase reveals key events in phosphorylation and Ca^{2+} release. *J. Biol. Chem.* **283,** 14867–14882
24. Beil, F. U., von Chak, D., and Hasselbach, W. (1977) Phosphorylation from inorganic phosphate and ATP synthesis of sarcoplasmic membranes. *Eur. J. Biochem.* **81,** 151–164
25. Punzengruber, C., Prager, R., Kolassa, N., Winkler, F., and Suko, J. (1978) Calcium gradient-dependent and calcium gradient-independent phosphorylation of sarcoplasmic reticulum by orthophosphate. The role of magnesium. *Eur. J. Biochem.* **92,** 349–359
26. Clarke, D. M., Loo, T. W., Inesi, G., and MacLennan, D. H. (1989) Location of high affinity Ca^{2+}-binding sites within the predicted transmembrane domain of the sarcoplasmic reticulum Ca^{2+}-ATPase. *Nature* **339,** 476–478
27. Toyoshima, C., Nakasako, M., Nomura, H., and Ogawa, H. (2000) Crystal structure of the calcium pump of sarcoplasmic reticulum at 2.6-Å resolution. *Nature* **405,** 647–655
28. Shinoda, T., Ogawa, H., Cornelius, F., and Toyoshima, C. (2009) Crystal structure of the sodium-potassium pump at 2.4-Å resolution. *Nature* **459,** 446–450